5734 *Biochemistry* **2010,** *49,* 5734–5742
DOI: 10.1021/bi100536t

BIOCHEMISTRY
including biophysical chemistry & molecular biology
Article

Interaction of Selective Serotonin Reuptake Inhibitors with Neuronal Nicotinic Acetylcholine Receptors[†]

Hugo R. Arias,*[,‡] Dominik Feuerbach,[§] Katarzyna M. Targowska-Duda,[∥] Megan Russell,[‡] and Krzysztof Jozwiak[∥]

[‡]*Department of Pharmaceutical Sciences, College of Pharmacy, Midwestern University, Glendale, Arizona 85308,* [§]*Neuroscience Research, Novartis Institutes for Biomedical Research, Basel, Switzerland, and* [∥]*Department of Chemistry, Medical University of Lublin, Lublin, Poland*

Received April 9, 2010; Revised Manuscript Received June 7, 2010

ABSTRACT: We compared the interaction of fluoxetine and paroxetine, two selective serotonin reuptake inhibitors (SSRIs), with the human (h) α4β2, α3β4, and α7 nicotinic acetylcholine receptors (AChRs) in different conformational states, using Ca^{2+} influx, radioligand binding, and molecular docking approaches. The results established that (1) fluoxetine was more potent than paroxetine in inhibiting agonist-activated Ca^{2+} influx on hα4β2 and hα7 AChRs, whereas the potency of both SSRIs was practically the same in the hα3β4 AChR. However, paroxetine was more potent in the hα7 AChR. (2) SSRIs bind to the [^{3}H]imipramine locus with higher affinity when the AChRs are in the desensitized states compared to the resting states. (3) The different receptor specificity for fluoxetine determined by their inhibitory potencies or binding affinities suggests different modes of interaction when the AChR is in the closed or activated state. (4) Neutral and protonated fluoxetine interacts with a binding domain located in the middle of the AChR ion channel. In conclusion, SSRIs inhibit the most important neuronal AChRs with potencies and affinities that are clinically relevant by binding to a luminal site that is shared with tricyclic antidepressants.

Clinical depression is a chronic illness that affects approximately 5−8% of the population of American adults or ∼15 million people each year (*1*). This common mental health disorder is one of the leading causes of disability in the United States and other countries. Although we do not have a clear view of the causes underlying mental depression, genetic and/or epigenetic factors might be involved (*2*). The latest evidence from brain imaging studies argues in favor of a familial component in the development of this disease (*3*). More specifically, the results indicate that the cortical thickness of right brain hemispheres from nondepressed persons with a family history of depression (high-risk group) was thinner than that from persons without a family history of depression (low-risk group). Fortunately, depression is a central nervous system disorder where the symptoms may diminish or disappear completely after proper treatment. Structurally and functionally different antidepressants are currently used with great clinical success. Among the most widely used are selective serotonin reuptake inhibitors (SSRIs),[1] including phenoxyphenylalkylamine derivatives such as fluoxetine, paroxetine, citalopram, and escitalopram, and phenylalkylamine derivatives such as sertraline and fluvoxamine (reviewed in ref *4*).

The main mechanism of action of SSRIs is to inhibit the transport of the neurotransmitter serotonin [5-hydroxytryptamine (5-TH)] into the presynaptic neuron, increasing the synaptic concentration of 5-HT, and finally enhancing the activity of postsynaptic 5-HT receptors. Nevertheless, SSRIs pharmacologically also behave as noncompetitive antagonists (NCAs) of several nicotinic acetylcholine receptors (AChRs) (*5*−*12*) (reviewed in ref *13*). AChRs are members of the Cys-loop ligand-gated ion channel superfamily that also includes γ-aminobutyric acid types A and C, type 3 5-HT, and glycine receptors (reviewed in refs (*13*−*15*)). An increasing amount of evidence suggests a possible role of neuronal AChRs in the process of depression as well as in the clinical activity of antidepressants (reviewed in refs *16* and *17*). The cholinergic-adrenergic theory is one of the accepted hypotheses used to describe the mechanisms of depression. This theory is based on the fact that hyperactivity or hypersensitivity of the cholinergic system over the adrenergic system can lead to depressed mood states (reviewed in ref *17*). Moreover, a higher rate of smokers is found in depressed patients compared with the general population (reviewed in ref *18*); mecamylamine, an unspecific NCA, weakens the symptoms of major depression (*19*), and nicotine as well as competitive antagonists and NCAs (e.g., mecamylamine) potentiates the antidepressant activity of imipramine and citalopram (*20*, *21*). Considering that the hyperactivity of the cholinergic system might be provoked by excessive neuronal AChR stimulation, the therapeutic action of

[†]This research was supported by grants from the Science Foundation Arizona and Stardust Foundation, the Office of Research and Sponsored Programs and the Master in Biomedical Sciences Program, Midwestern University (to H.R.A.), and by the Polish Ministry of Science and Higher Education (N405 297036) and The Foundation for Polish Science (TEAM program) (to K.J.). M.R. was supported by the Master in Biomedical Sciences Program, Midwestern University.

*To whom correspondence should be addressed: Department of Pharmaceutical Sciences, College of Pharmacy, Midwestern University, 19555 N. 59th Ave., Glendale, AZ 85308. Telephone: (623) 572-3589. Fax: (623) 572-3550. E-mail: harias@midwestern.edu.

[1]Abbreviations: AChR, nicotinic acetylcholine receptor; NCA, noncompetitive antagonist; SSRIs, selective serotonin reuptake inhibitors; fluoxetine, (±)-*N*-methyl-γ-[4-(trifluoromethyl)phenoxy]benzenepropanamine; paroxetine, (3*S*-*trans*)-3-[(1,3-benzodioxol-5-yloxy)methyl]-4-(4-fluorophenyl)piperidine; κ-BTx, κ-bungarotoxin; α-BTx, α-bungarotoxin; RT, room temperature; BS, binding saline; K_i, inhibition constant; K_d, dissociation constant; IC_{50}, ligand concentration that inhibits 50% of binding or Ca^{2+} influx; n_H, Hill coefficient; DMEM, Dulbecco's modified Eagle's medium; FBS, fetal bovine serum; BSA, bovine serum albumin.

 Published on Web 06/09/2010

many antidepressants may be mediated in part through inhibition of one or more AChRs.

Considering these results, possible roles for neuronal AChRs as targets for the beneficial action elicited by SSRIs can be suggested. Thus, a better understanding of the interaction of SSRIs with AChRs is crucial to the development of new analogues for safer antidepressant therapies or even for novel clinical uses. For instance, fluoxetine has been used, although it is not approved by the FDA, for the treatment of obsessive-compulsive, panic, and premenstrual dysphoric disorders, as well as in drug addiction and bulimia (e.g., see ref *22*). In this regard, we want to characterize the interaction of fluoxetine and paroxetine with the most prominent AChRs in the brain, including the human (h) α4β2, hα3β4, and hα7 AChRs, each subtype in different conformational states. To accomplish these objectives, we will use structural and functional approaches, including radioligand competition binding assays using [^{3}H]imipramine as a probe for the antidepressant site, Ca^{2+} influx-induced fluorescence measurements, and molecular modeling and docking studies.

EXPERIMENTAL PROCEDURES

Materials. [^{3}H]Imipramine (47.5 Ci/mmol) was obtained from PerkinElmer Life Sciences Products, Inc. (Boston, MA), and stored in ethanol at −20 °C. Imipramine hydrochloride, fluoxetine {(±)-*N*-methyl-γ-[4-(trifluoromethyl)phenoxy]benzenepropanamine} hydrochloride, paroxetine {(3*S*-*trans*)-3-[(1,3-benzodioxol-5-yloxy)methyl]-4-(4-fluorophenyl)piperidine} hydrochloride hemihydrate, polyethylenimine, leupeptin, bacitracin, pepstatin A, aprotinin, benzamidine, and phenylmethanesulfonyl fluoride were purchased from Sigma Chemical Co. (St. Louis, MO). (±)-Epibatidine hydrochloride, Geneticin, and hygromycin B were obtained from Tocris Bioscience (Ellisville, MO). κ-Bungarotoxin (κ-BTx) was obtained from Biotoxins Inc. (St. Cloud, FL). α-Bungarotoxin (α-BTx) was obtained from Invitrogen Co. (Carlsbad, CA). Fetal bovine serum (FBS) and trypsin/EDTA were purchased form Gibco BRL (Paisley, U.K.). Salts were of analytical grade.

Cell Culture Procedures. HEK293-hα3β4 and HEK293-hα4β2 cell lines were cultured as previously described (*23*−*25*). In brief, cells were cultured in a 1:1 mixture of Dulbecco's modified Eagle's medium containing 3.7 g/L $NaHCO_3$, 1.0 g/L sucrose, stable glutamine (L-alanyl-L-glutamine, 524 mg/L), and Ham's F-12 nutrient mixture (Invitrogen, Paisley, U.K.) containing 1.176 g/L $NaHCO_3$ and supplemented with 10% (v/v) FBS, Geneticin (0.2 mg/mL), and hygromycin B (0.2 mg/mL). GH3-hα7 cells were cultured in Ham's F-12 nutrient mixture containing 1.176 g/L $NaHCO_3$ and 524 mg/L stable glutamine and supplemented with 10% (v/v) FBS and 50 μg/mL Geneticin. SHSY5Y-hα7 cells were cultured in Dulbecco's modified Eagle's medium supplemented with 10% (v/v) FBS and 100 μg/mL Geneticin. All different cells were cultured at 37 °C, 5% CO_2, and 95% relative humidity. Cells were passed every 3 days via detachment of the cells from the cell culture flask by a brief incubation (~3 min) with trypsin (0.5 mg/mL)/EDTA (0.2 mg/mL) after the cells had been washed with phosphate-buffered saline.

Ca^{2+} Influx Measurements. Ca^{2+} influx was assessed as previously described (*11*, *12*, *23*−*26*). Briefly, 5×10^4 GH3-hα7, HEK293-hα3β4, and HEK293-hα4β2 cells per well were seeded 72 h prior to the experiment on black 96-well plates (Costar, New York, NY) and incubated at 37 °C in a humidified atmosphere (5% CO_2/95% air); 16−24 h before the experiment, the medium was changed to 1% bovine serum albumin in HEPES-buffered salt solution (HBSS) [130 mM NaCl, 5.4 mM KCl, 2 mM $CaCl_2$, 0.8 mM $MgSO_4$, 0.9 mM NaH_2PO_4, 25 mM glucose, and 20 mM HEPES (pH 7.4)]. On the day of the experiment, the medium was removed by flicking the plates and replaced with 100 μL of HBSS and 1% bovine serum albumin containing 2 μM Fluo-4 (Molecular Probes, Eugene, OR) in the presence of 2.5 mM probenecid (Sigma, Buchs, Switzerland). The cells were then incubated at 37 °C in a humidified atmosphere (5% CO_2/95% air) for 1 h. Plates were flicked to remove excess of Fluo-4, washed twice with HBSS and 1% bovine serum albumin, and finally refilled with 100 μL of HBSS containing different concentrations of fluoxetine or paroxetine and preincubated for 5 min. Plates were then placed in the cell plate stage of the fluorescent imaging plate reader (Molecular Devices, Sunnyvale, CA). A baseline consisting of five measurements of 0.4 s each was recorded. (±)-Epibatidine (0.1 μM) was then added from the agonist plate to the cell plate using the 96-tip pipettor simultaneously to record fluorescence for a total length of 3 min. The laser excitation and emission wavelengths are 488 and 510 nm, respectively, at 1 W, and a CCD camera opening of 0.4 s.

Preparation of Native Membranes from Cells Expressing Specific AChR Subtypes. To prepare cell membranes in large quantities, HEK293-hα3β4, HEK293-hα4β2, and SH-SY5Y-hα7 cells were cultured separately in suspension using nontreated Petri dishes (150 mm × 15 mm) as previously described (*12*, *24*−*26*). After the cells had been cultured for ~2−3 weeks, cells were harvested via gentle scraping and centrifuged at 1000 rpm for 5 min at 4 °C using a Sorvall Super T21 centrifuge. Cells were resuspended in binding saline (BS) buffer [50 mM Tris-HCl, 120 mM NaCl, 5 mM KCl, 2 mM $CaCl_2$, and 1 mM $MgCl_2$ (pH 7.4)] containing 0.025% (w/v) sodium azide and a cocktail of protease inhibitors, including leupeptin, bacitracin, pepstatin A, aprotinin, benzamidine, and phenylmethanesulfonyl fluoride. The suspension was maintained on ice and homogenized using a Polytron PT3000 instrument (Brinkmann Instruments Inc., Westbury, NY) and then centrifuged at 10000 rpm for 30 min at 4 °C. The pellet was finally resuspended in BS buffer containing 20% sucrose (w/v) using the Polytron and briefly (5 × 15 s) sonicated (Branson Ultrasonics Co., Danbury, CT) to ensure maximum homogenization. Cell membranes containing hα7, hα4β2, or hα3β4 AChRs were frozen at −80 °C until they were required. Total protein was determined using the bicinchoninic acid protein assay (Thermo Fisher Scientific, Rockford, IL).

[^{3}H]Imipramine Competition Binding Experiments Using Neuronal AChRs in Different Conformational States. We compared the effect of fluoxetine and paroxetine on the binding of [^{3}H]imipramine to hα4β2, hα3β4, and hα7 AChRs in different conformational states using a method previously developed (*24*, *25*). In this regard, AChR membranes (1.5 mg/mL) were suspended in BS buffer with 13 nM (hα4β2 and hα3β4 AChR membranes) or 17 nM (hα7 AChR membranes) [^{3}H]imipramine in the absence (resting and no ligand) or presence of 0.1 μM κ-bungarotoxin (κ-BTx) (hα4β2 and hα3β4 AChR membranes) or α-bungarotoxin (α-BTx) (resting or BTx-bound state), or alternatively in the presence of 0.5 μM (±)-epibatidine (desensitized and agonist-bound state), and preincubated for 30 min at RT. Bungarotoxins are competitive antagonists that maintain the AChRs in the resting (closed) state (*27*). Nonspecific binding was assessed in the presence of 100 μM imipramine.

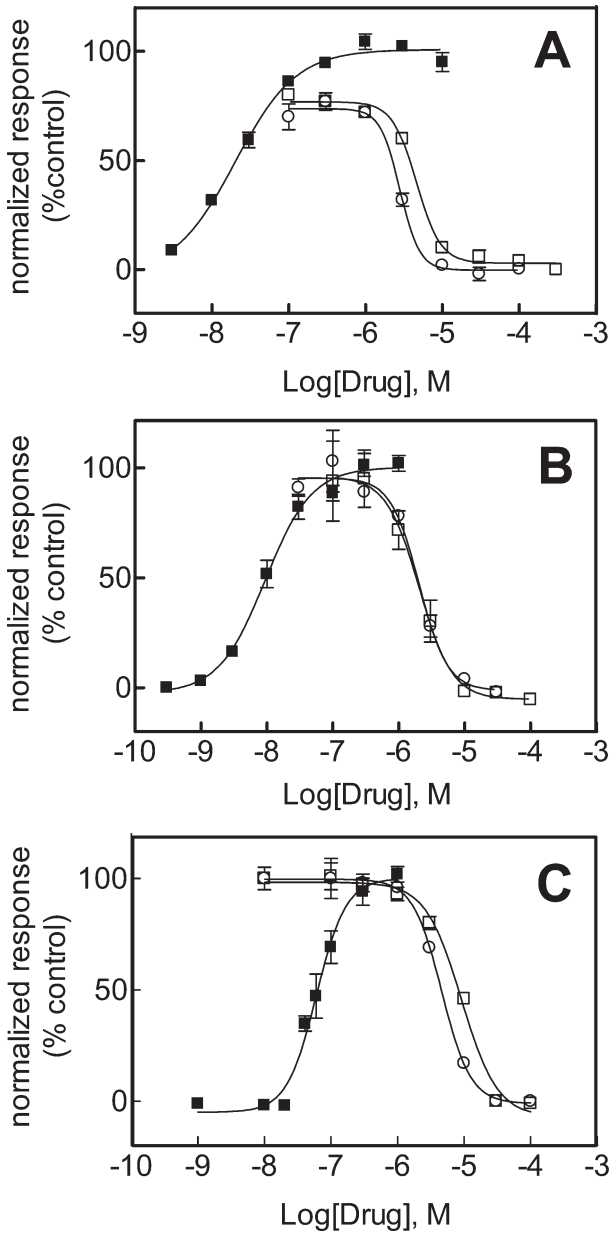

FIGURE 1: Inhibitory effect of SSRIs on (±)-epibatidine-induced Ca^{2+} influx in (A) HEK293-hα4β2, (B) HEK293-hα3β4, and (C) GH3-hα7 cells. Increased concentrations of (±)-epibatidine (■; n = 28) activate the AChRs with potencies (EC_{50} values in nanomolar): 30 ± 5 (hα4β2), 19 ± 7 (hα3β4), and 52 ± 4 (hα7), respectively. df/f values of 1.19 ± 0.08, 1.67 ± 0.23, and 0.64 ± 0.23 were obtained for the assays using the HEK293-hα4β2, HEK293-hα3β4, and GH3-hα7 cells, respectively. Subsequently, cells were pretreated with several concentrations of fluoxetine (○) and paroxetine (□), followed by addition of 0.1 μM (±)-epibatidine. The response was normalized to the maximal (±)-epibatidine response which was set to 100%. The plots are representative of at least four determinations, where the error bars correspond to the standard deviation. The calculated IC_{50} and n_H values are summarized in Table 1.

The total volume was divided into aliquots, and increasing concentrations of the ligand under study were added to each tube and incubated for 2 h at RT. AChR-bound radioligand was then separated from free ligand by a filtration assay using a 48-sample harvester system with GF/B Whatman filters (Brandel Inc., Gaithersburg, MD), previously soaked with 0.5% polyethylenimine for 30 min. The membrane-containing filters were transferred to scintillation vials with 3 mL of Bio-Safe II (Research Product International Corp., Mount Prospect, IL), and the radioactivity was determined using a Beckman LS6500 scintillation counter (Beckman Coulter, Inc., Fullerton, CA).

Table 1: Inhibitory Potencies of SSRIs for the hα4β2, hα3β2, and hα7 AChRs

AChR subtype	SSRI	IC_{50} (μM)[a]	n_H[b]	no. of experiments (n)
hα4β2	fluoxetine	4.4 ± 0.6	2.10 ± 0.17	8
	paroxetine	8.6 ± 2.3	1.85 ± 0.10	4
hα3β4	fluoxetine	2.0 ± 0.4	1.67 ± 0.26	5
	paroxetine	2.6 ± 0.3	1.62 ± 0.29	6
hα7	fluoxetine	4.9 ± 1.0	1.44 ± 0.37	4
	paroxetine	8.6 ± 2.0	1.64 ± 0.28	9

[a] IC_{50} values were obtained from panels A (hα4β2), B (hα3β4), and C (hα7) of Figure 1, according to eq 1. [b] Hill coefficient.

The concentration−response data were curve-fitted by nonlinear least-squares analysis using Prism. The corresponding IC_{50} values were calculated using the following equation:

$$0 = 1/[1 + ([L]/IC_{50})^{n_H}] \quad (1)$$

where θ is the fractional amount of the radioligand bound in the presence of inhibitor at a concentration [L] compared to the amount of the radioligand bound in the absence of inhibitor (total binding). IC_{50} is the inhibitor concentration at which θ = 0.5 (50% bound), and n_H is the Hill coefficient. The IC_{50} and the n_H values obtained from the radioligand competition experiments in the desensitized state are summarized in Table 2.

The observed IC_{50} values from the competition experiments described above were transformed into inhibition constant (K_i) values using the Cheng−Prusoff relationship (*28*):

$$K_i = IC_{50}/(1 + [[^3H]\text{imipramine}]/K_d^{\text{imipramine}}) \quad (2)$$

where [[^{3}H]imipramine] is the initial concentration of [^{3}H]imipramine and $K_d^{\text{imipramine}}$ is the [^{3}H]imipramine dissociation constant for the hα3β4 [0.41 μM (*24*)], hα4β2 [0.83 μM (*25*)], and hα7 [1 μM (H. R. Arias et al., manuscript in preparation)] AChRs, respectively.

Molecular Docking of Fluoxetine in the hα4β2, hα3β4, and hα7 AChR Ion Channels. Since the absolute numbering of amino acid residues varies greatly between AChR subunits, the residues in the M2 transmembrane segments (responsible for interactions with fluoxetine) from the α3, α4, α7, β2, and β4 subunits are named here using the prime nomenclature (1′−20′), corresponding to residues Met^{243}−Glu^{262} of the *Torpedo* α1 subunit. As seen in Figure 3A, the sequences of the M2 segments are considerably different among the studied subunits. Interestingly, the subunits differ in the position in which residues are regarded to be exposed to the center of the channel and are found to be important in interactions with NCAs. For example, the α7 subunit carries Ser residues at position 2′ and Thr residues at position 6′, whereas the other studied subunits contain Thr residues at position 2′ and Ser residues at position 6′. Similarly, the β4 subunit has Phe residues at position 13′, whereas other subunits contain Val residues in this position. Finally, the β2 and β4 subunits contain Lys residues at position 20′, while the α3, α4, and α7 subunits carry Glu residues in the same position. These differences in residues forming rings along the axis of the channel for the studied subtypes were found to be important in the docking simulation results where certain subtype specific interactions were modeled as described in Results.

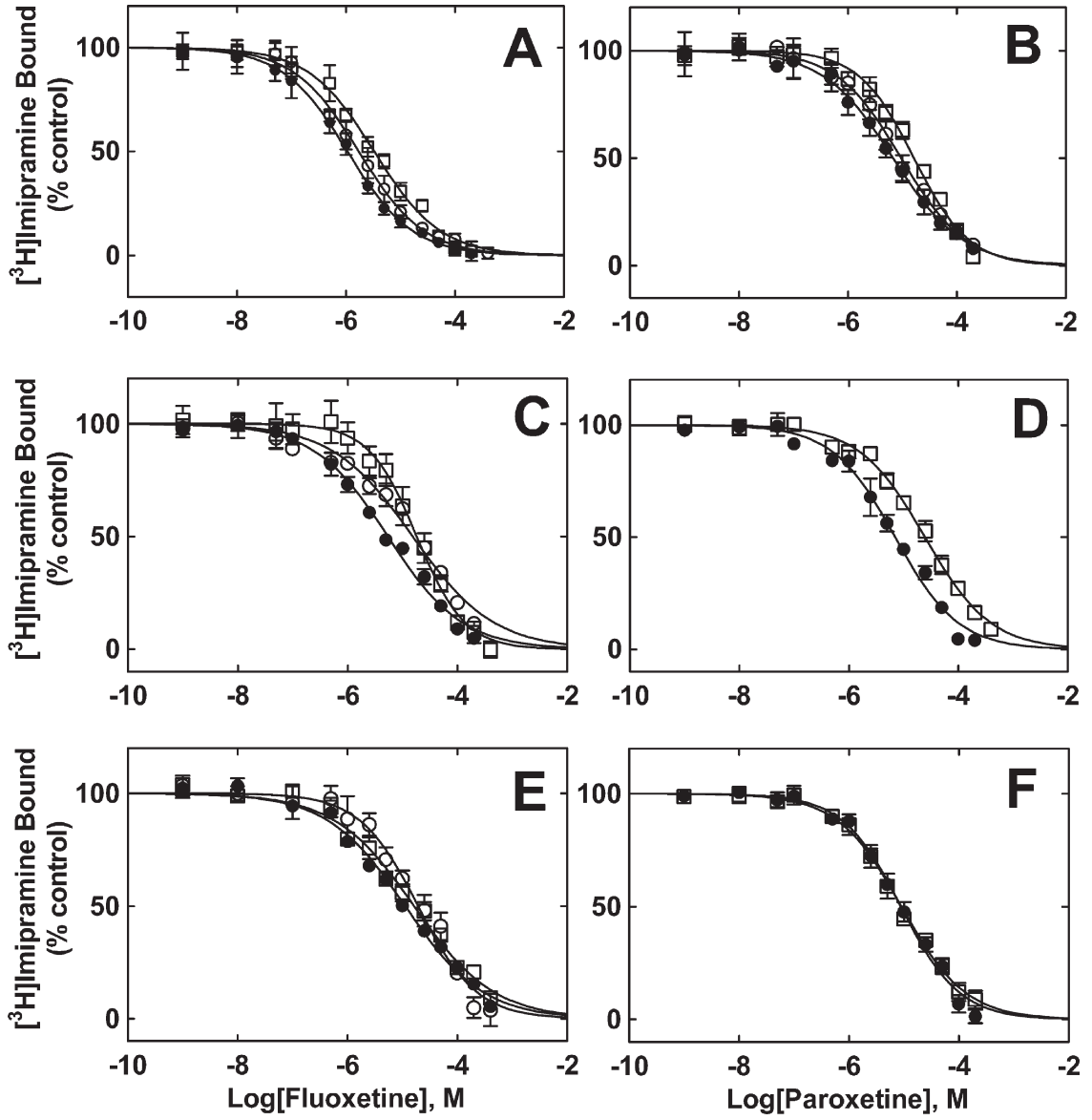

FIGURE 2: Inhibition of [^{3}H]imipramine binding to nuronal AChRs in different conformational states by fluoxetine and paroxetine. h$\alpha 4\beta 2$ (A and B), h$\alpha 3\beta 4$ (C and D), and h$\alpha 7$ (E and F) AChR-containing membranes (1.5 mg/mL) were equilibrated (2 h) with 13 (for h$\alpha 4\beta 2$ and h$\alpha 3\beta 4$) or 17 (for h$\alpha 7$) nM [^{3}H]imipramine in the absence (○) or presence of 0.1 μM κ-BTx (□) (resting state) and in the presence of 0.5−1 μM (±)-epibatidine (●) (desensitized state), respectively, and increasing concentrations of fluoxetine or paroxetine. Nonspecific binding was assessed at 100 μM imipramine. Each plot is the combination of two to four separate experiments each performed in triplicate, where the error bars correspond to the standard deviation. From these plots, the IC_{50} and n_H values were obtained by nonlinear least-squares fit according to eq 1. Subsequently, the K_i values were calculated using eq 2 and summarized in Table 2.

Computational simulations were performed using the same protocol as recently reported (*24*−*26*, *29*). Molecular models of the transmembrane domain of h$\alpha 4\beta 2$, h$\alpha 3\beta 4$, and h$\alpha 7$ AChRs were constructed using homology/comparative modeling method employing the *Torpedo* AChR structure (*30*, *31*) [Protein Data Bank (PDB) entry 2BG9] as a template. Fluoxetine and paroxetine molecules (both in the neutral and protonated states) were prepared using HyperChem 6.0 (HyperCube Inc., Gainesville, FL). Sketched molecules were optimized using semiempirical method AM1 (Polak-Ribiere algorithm to a gradient lower than 0.1 kcal $Å^{-1}$ mol^{-1}) and then transferred for the subsequent step of ligand docking. The Molegro Virtual Docker (MVD 2010.4.0.0, Molegro ApS, Aarhus, Denmark) was used for docking simulations of flexible ligands into the rigid target AChR model. In this step, the complete structures of target receptors were used. The docking space was limited and centered in the middle of the ion channel and extended enough to ensure coverage of the whole channel domain for sampling simulations (docking space was defined as a sphere 21 Å in diameter). The actual docking simulations were performed using the following settings: number of runs being 100, maximal number of iterations being 10000, and maximal number of poses being 10. The poses representing the lowest value of the scoring function (MolDockScore) for fluoxetine and paroxetine were further analyzed.

RESULTS

SSRI-Induced Inhibition of (±)*-Epibatidine-Mediated* Ca^{2+} *Influx in AChR-Expressing Cells*. The potencies of (±)-epibatidine in activating the h$\alpha 4\beta 2$, h$\alpha 3\beta 4$, and h$\alpha 7$ AChRs were first determined by assessing the fluorescence change in HEK293-h$\alpha 4\beta 2$, HEK293-h$\alpha 3\beta 4$, and GH3-h$\alpha 7$ cells after (±)-epibatidine stimulation. In these Ca^{2+} influx experiments, we obtained practically the same signal-to-noise ratio as those

published previously for the three cell lines (*11*, *23*). To assess the quality and robustness of the assays, which depend on the signal-to-noise ratio and variability, the treatment control/control ratio (d*f*/*f*) was calculated for each cell line. d*f*/*f* is a dimension-less number, where values below 0.5 indicate that the assay presents low signal-to-noise ratios, values between 0.5 and 1.0 are evidence of good quality assays, and values above 1 are evidence of extremely robust assays. For the maximal (±)-epibatidine response, values of 1.19 ± 0.08, 1.67 ± 0.23, and 0.64 ± 0.23 were obtained for the assays using the HEK293-hα4*β*2, HEK293-hα3*β*4, and GH3-hα7 cells, respectively, indicating that our results can be considered of good and excellent quality.

The observed EC_{50} values for the hα4*β*2 [30 ± 5 nM (Figure 1A)], hα3*β*4 [19 ± 7 nM (Figure 1B)], and hα7 [52 ± 4 nM (Figure 1C)] AChR are in the same concentration range as those previously determined using cell lines expressing the same AChR types (*11*, *23*−*25*, *32*). Preincubation with SSRIs blocked subsequently the activation elicited by (±)-epibatidine on the hα4*β*2 (Figure 1A), hα3*β*4 (Figure 1B), and hα7 (Figure 1C) AChRs, respectively. The calculated IC_{50} values for the SSRIs indicate that fluoxetine is more potent than paroxetine in inhibiting the hα4*β*2 and hα7 AChRs, but the potency is similar for the hα3*β*4 AChR (Table 1). On the basis of the observed inhibitory potencies, the order of the receptor specificities for SSRIs is as follows: hα3*β*4 > hα4*β*2 > hα7 (Table 1). The fact that the n_H values for SSRIs are higher than unity, and even two for the case of the hα4*β*2 AChR (Table 1), indicates that the blocking process mediated by these antidepressants is produced in a cooperative manner.

[^{3}H]Imipramine Binding Competition Experiments Using hα4β2, hα3β4, and hα7 AChRs in Different Conformational States. The binding affinity of SSRIs for the hα4*β*2, hα3*β*4, and hα7 AChRs in different conformational states was studied by radioligand competition experiments. In this regard, the effects of fluoxetine and paroxetine on [^{3}H]imipramine binding to hα4*β*2 (Figure 2A,B), hα3*β*4 (Figure 2C,D), and hα7 (Figure 2E,F) AChRs in the resting (BTx-bound) and desensitized (agonist-bound) states were determined. The [^{3}H]imipramine binding levels for each AChR subtype depended on the membrane preparation and ranged between 2000 and 4000 dpm and between 500 and 1000 dpm for the total and nonspecific binding, respectively. Each SSRI inhibits ∼100% of the specific binding of [^{3}H]imipramine to either AChR type in either conformational state. The first observation is that SSRIs present higher specificity for the hα4*β*2 AChR compared to that for the hα7 and hα3*β*4 AChRs (Table 2). The second observation is that in general, fluoxetine has a higher affinity than paroxetine for each AChR subtype, except for the hα7 AChR where paroxetine has an affinity higher than that for fluoxetine (Table 2). The third observation is that the affinity of SSRIs for the desensitized AChRs (in the presence of agonists) is higher than that for the resting AChRs (in the presence of BTxs). This suggests that SSRIs may discriminate between the desensitized and resting conformational states of neuronal AChRs. The exception is paroxetine on the hα7 AChR, where the binding affinity in the resting and desensitized states is practically the same. The fourth observation is that the affinity of SSRIs for the hα4*β*2 AChR pretreated with κ-BTx is lower than that obtained without the neurotoxin, whereas the values are similar for the hα3*β*4 and the hα7 AChRs (Table 2). This suggests that the hα4*β*2 AChR membrane preparation contains a portion of desensitized AChRs, whereas the hα3*β*4 and hα7 AChR membranes contain AChRs that are mainly in the resting state. The final observation is that the calculated n_H values are close to unity (Table 2), indicating that the SSRIs inhibit [^{3}H]imipramine binding in a noncooperative manner. This result suggests that SSRIs interact with a single binding site in each AChR ion channel or with several sites with similar affinity. In turn, this evidence suggests that SSRIs may be interacting with the [^{3}H]imipramine binding site in a steric fashion.

Table 2: Binding Affinities of SSRIs for the [^{3}H]Imipramine Binding Site at the hα4*β*2, hα3*β*4, and hα7 AChRs

		resting state		desensitized state	
AChR type	SSRI	K_i (μM)	n_H[e]	K_i[d] (μM)	n_H[e]
hα4*β*2	fluoxetine	1.7 ± 0.3[a]	0.73 ± 0.08	1.0 ± 0.1	0.73 ± 0.04
		3.2 ± 0.4[b]	0.72 ± 0.06		
	paroxetine	9.4 ± 1.2[a]	0.73 ± 0.07	6.7 ± 0.9	0.68 ± 0.06
		16.1 ± 1.3[b]	0.86 ± 0.05		
hα3*β*4	fluoxetine	17.5 ± 2.2[a]	1.00 ± 0.11	4.8 ± 0.5	0.63 ± 0.04
		14.9 ± 1.4[b]	0.60 ± 0.04		
	paroxetine	24.0 ± 1.8[a]	0.72 ± 0.04	6.9 ± 0.6	0.76 ± 0.05
hα7	fluoxetine	18.8 ± 2.5[a]	0.83 ± 0.08	11.0 ± 1.0	0.61 ± 0.03
		16.9 ± 1.4[c]	0.63 ± 0.03		
	paroxetine	8.9 ± 0.8[c]	0.75 ± 0.05	8.7 ± 0.6	0.82 ± 0.04

[a]Obtained in the absence of κ-BTx. [b]Obtained in the presence of κ-BTx. [c]Obtained in the presence of α-BTx (Figure 2A−F), according to eq 2. [d]The K_i values in the desensitized state were obtained in the presence of (±)-epibatidine (Figure 2A−F), according to eq 2. [e]Hill coefficient.

Molecular Docking of Fluoxetine in the hα4β2, hα3β4, and hα7 AChR Ion Channels. Fluoxetine, in the neutral and protonated states, was docked to the hα4*β*2, hα3*β*4, and hα7 AChR ion channel models using Molegro Virtual Docker version 2010.4.0.0. To determine the structural basis of the observed higher affinity of paroxetine compared to that for fluoxetine in the hα7 AChR (see Table 2), additional docking experiments were performed for paroxetine. Each simulation generated a series of docking poses and ranked them using energy-based criteria using the embedded scoring function, MolDockScore (see Table 3). On the basis of this ranking, the lowest-energy pose of the ligand−receptor complex was selected and presented in panels B (hα4*β*2), C (hα7), and D (hα3*β*4) of Figure 3.

In general, fluoxetine in either the neutral or protonated state interacts within the middle portion of each channel with all five M2 helices, but not with other transmembrane segments (Figure 3B). The molecule binds to a domain formed between amino acid rings at positions 6′ and 13′. Orientations of docked fluoxetine in the hα4*β*2 (Figure 3B) and hα7 (Figure 3C) channel models are essentially the same. However, the orientation in the hα3*β*4 ion channel is slightly different. More specifically, the position of the fluoxetine benzyl ring in this ion channel (see Figure 3D) is exchanged with the position of the aminoaryl moiety determined in the other AChR subtypes (see Figure 3B,C).

MolDockScore values for the hα3*β*4 AChR are the lowest among all tested AChR subtypes (see Table 3), indicating that the interaction of fluoxetine with the hα3*β*4 AChR is the most stable among those of the studied AChR subtypes. This is in agreement with the higher inhibitory potency of fluoxetine for the hα3*β*4 AChR compared to that for the other neuronal AChR subtypes (see Table 1). In addition, paroxetine has lower MolDockScore values than fluoxetine for the hα7 AChR (see Table 3), which is in agreement with the higher affinity of paroxetine compared with that for fluoxetine (see Table 1).

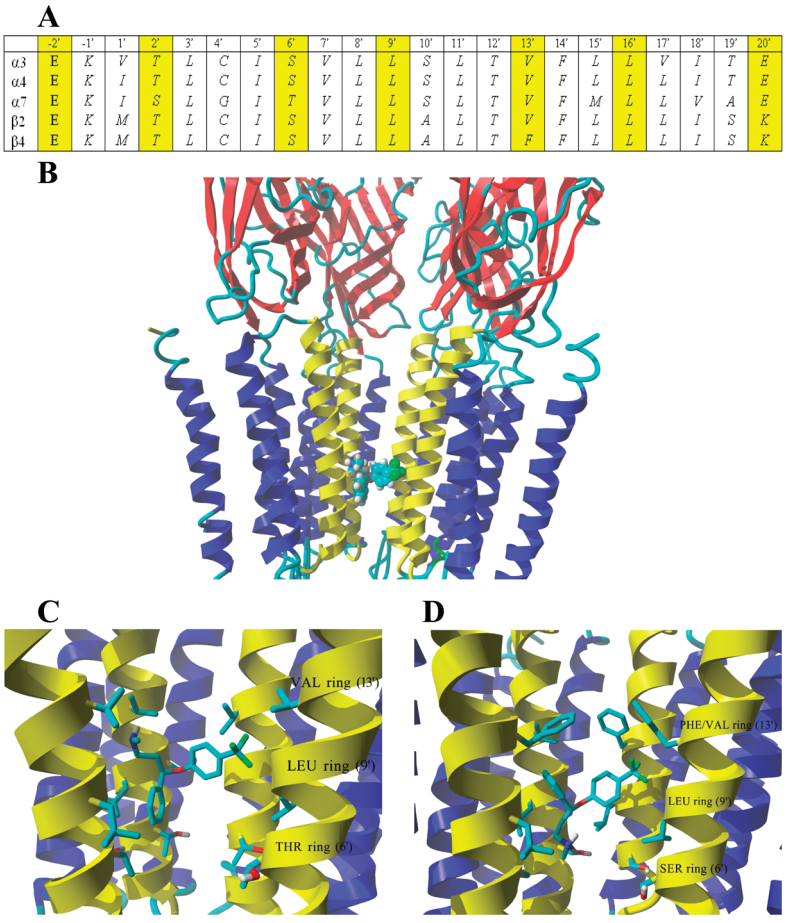

FIGURE 3: Molecular docking of fluoxetine in the hα4β2, hα7, and hα3β4 AChR ion channels. (A) Sequence alignment of M2 helical segments for the subunits forming the studied AChR subtypes. Yellow boxes show the residues exposed to the center of the ion channel and forming the amino acid rings shown in the following models. (B) Side view of the lowest-energy complex formed between protonated fluoxetine (rendered in element color-coded ball mode) and the hα4β2 AChR ion channel. The molecule interacts with the middle portion of all five M2 helices but not with other transmembrane segments. The orientation of neutral fluoxetine docked into the hα4β2 ion channel model is the same. Part of the receptor extracellular portion is also shown to have a better perspective of the fluoxetine binding site location. (C) Detailed interaction of protonated fluoxetine with the domain formed between the amino acid rings at positions 6′ and 13′ in the hα7 AChR ion channel by van der Waals and hydrogen bond interactions. The orientation of neutral fluoxetine docked into the hα7 ion channel model is the same. (D) Detailed interaction of neutral fluoxetine with the domain formed between the amino acid rings at positions 6′ and 13′ in the hα3β4 AChR ion channel by van der Waals and hydrogen bond interactions. The position of the fluoxetine benzyl ring in this ion channel is exchanged with the position of the aminoaryl moiety determined in the other AChR subtypes (see panels B and C). As a consequence, both aromatic rings of the fluoxetine molecule bind to the three Phe residues at position 13′ (β4-Phe253) probably by $\pi-\pi$ interactions. The orientation of protonated fluoxetine docked into the hα3β4 ion channel model is the same. In panels C and D, M2 transmembrane helices forming the wall of the channel are colored yellow and all other transmembrane segments are colored blue. Residues from each ring are shown explicitly in stick mode. The fluoxetine molecule is rendered in element color-coded stick mode. All nonpolar hydrogen atoms are hidden. For the sake of clarity, one subunit from each AChR subtype is hidden.

DISCUSSION

Pharmacologically, SSRIs behave as NCAs of several AChRs (*5*−*12*) (reviewed in refs *13* and *17*). This and additional evidence supports the view that neuronal AChRs might be targets for the clinical activity of SSRIs, one of the antidepressants used most widely worldwide (reviewed in ref *17*). In this regard, we want to determine the receptor specificity, affinity, inhibitory potency, and structural components for the interaction of fluoxetine and paroxetine with the most important and prominent AChRs in the brain, including the hα4β2, hα3β4, and hα7 AChR subtypes. To accomplish these objectives, we will use structural and functional approaches, including radioligand competition binding assays using [^{3}H]imipramine as a probe for the antidepressant site, Ca^{2+} influx-induced fluorescence measurements, and molecular modeling and docking studies.

Functional Aspects of SSRIs Interacting with Neuronal AChRs. To determine the effect of SSRIs on (±)-epibatidine-activated Ca^{2+} influx in HEK293-hα4β2 (Figure 1A), HEK293-hα3β4 (Figure 1B), and GH3-hα7 (Figure 1C) cells, we used a preincubation protocol. In general, fluoxetine (IC_{50} range of 2.0−4.9 μM) was more potent than paroxetine (IC_{50} range of 2.6−11.3 μM) in inhibiting the respective AChRs (see Table 1). Previous studies showed that fluoxetine and paroxetine inhibit the hα3β4 (*10*) and hα7 (*11*) AChRs with practically the same potencies as those obtained in this study. Considering our data (see Table 1) and the IC_{50} values for fluoxetine obtained in the human embryonic muscle and chick mutated AChRs (*10*, *12*), the order of inhibitory receptor specificities is as follows (IC_{50} values in micromolar): hα1β1γδ (1.8−2.1) ∼ hα3β4 (2.0) > hα4β2 (4.4) > hα7 (4.9) > V274T-chick α7 (11.2).

In general, the observed n_H values for fluoxetine and paroxetine are higher than unity, and even near two in the case of paroxetine-induced inhibition of the hα3β4 AChR (see Table 1). Hill coefficients higher than unity were also observed for the hα3β4 (*10*) and hα1β1γδ (*12*) AChRs. These results suggest that

Table 3: MolDockScore Values for the Lowest Energy of SSRIs Complexed with the hα4β2, hα3β4, and hα7 AChR Ion Channels, Obtained by Molecular Docking[a]

AChR type	SSRI	molecular form	MolDockScore (kJ/mol)
hα4β2	fluoxetine	neutral	−109
		protonated	−105
hα3β4	fluoxetine	neutral	−125
		protonated	−127
hα7	fluoxetine	neutral	−116
		protonated	−118
	aroxetine	neutral	−129
		protonated	−132

[a]Molegro Virtual Docker generated a series of docking poses and ranked them using energy-based criteria using the embedded scoring function in MolDockScore. The table presents MolDockScore values calculated for the lowest-energy pose for each simulation; thus, no standard deviation can be provided.

there is potentially more than one binding site for these SSRIs in the activated AChR ion channels, especially in the case of the hα3β4 AChR, or, alternatively, that there is more than one mechanism of inhibition. For example, SSRI-induced AChR desensitization was observed in the *Torpedo* AChR (*12*).

At therapeutic doses, the plasma concentrations of fluoxetine and paroxetine have been determined to be in the range of ∼0.6 and ∼0.3 μM, respectively (reviewed in ref *33*). Moreover, higher concentrations of fluoxetine and its active metabolite have been detected in the brain using in vivo magnetic resonance spectroscopy imaging, reaching values as high as ∼30 μM (*34*, *35*). Considering that only 5−10% of this concentration is in the free, non-protein-bound, form, an active concentration of ∼3 μM can be reached in the brain. However, we must take into account the fact that the protein-bound and free forms are in dynamic equilibrium, and every time that a fraction of the free form is taken by the cell, the same fraction is dissociated from the protein-bound form to maintain the equilibrium. In this regard, the protein-bound form can be considered a drug reservoir, keeping the concentration of the active drug constant. In any case, these two SSRIs can produce appreciable AChR inhibition, more particularly on the hα3β4 AChR, with the subsequent clinical relevance of this activity, especially under long-term clinical treatment. In addition to ganglia, α3β4-containing AChRs are expressed in the medial habenula, interpeduncular nucleus, ventral tegmental area, dorsolateral tegmentum, basolateral amygdala, locus coeruleus, and hippocampus (*36*, *37*) (reviewed in refs *16* and *38*), where some of these brain areas are involved in mood regulation, anxiety-related responses, and drug reward (*36*, *37*) (reviewed in ref *39*).

Structural Aspects of SSRIs Interacting with Neuronal AChR Ion Channels. The results from the [^{3}H]imipramine competition binding experiments indicate that fluoxetine binds to the hα4β2 and hα3β4 AChRs, with an affinity higher than that for paroxetine, whereas the opposite is true for the hα7 AChR (see Table 2). In most cases, SSRIs bind to the ion channels with higher affinity when the AChRs are in the desensitized states compared to the resting states. This observation is more apparent in the case of the hα3β4 and hα4β2 AChRs, where fluoxetine binds with ∼3-fold higher affinity to the desensitized, agonist-bound AChR compared to the resting, κ-BTx-bound AChR (see Table 2). Moreover, larger differences in affinity binding were observed for SSRIs (∼18-fold) between resting and desensitized *Torpedo* AChRs (*12*), and in the inhibitory potency of fluoxetine (∼27-fold) between the activated and resting α7 AChRs (*9*). On the basis of these data, we can conclude that SSRIs may discriminate among the resting, activated, and desensitized states of different AChRs. Interestingly, although tricyclic antidepressants also discriminate between the desensitized and resting *Torpedo* AChRs (*29*, *40*), they do not differentiate very well the desensitized and resting states of the hα3β4 (*24*) and hα4β2 (*25*) AChRs. Another way of considering the inhibitory activity of SSRIs at the AChR would be to compare their affinities and potencies for the different conformational states of the receptor. Taking the hα4β2 AChR as an example, we can infer that fluoxetine interacts with the following relative affinities and potencies: desensitized (IC_{50} = 1.0 μM; see Table 2) > resting (K_i = 3.2 μM; see Table 2) > activated (IC_{50} = 4.4 μM; see Table 1). Considering our data for fluoxetine and the K_i value for fluoxetine obtained in the *Torpedo* AChR (i.e., α1β1γδ) (*12*), the order of AChR specificity in the resting state is as follows (K_i values in micromolar): hα4β2 (1.8) ∼ α1β1γδ (1.9) > hα3β4 (14.9) > hα7 (16.9). This order is perfectly maintained in the desensitized state as well: hα4β2 (1.0) ∼ α1β1γδ (0.96) > hα3β4 (4.8) > hα7 (11.0).

The observed n_H values from the competition binding experiments are close to unity (see Table 2), suggesting that SSRIs may be interacting with the [^{3}H]imipramine binding site in a steric fashion. These results support the idea that the SSRI binding site overlaps the imipramine locus in both the desensitized and resting AChR ion channels. Previous competition binding results for the *Torpedo* AChR suggest that SSRIs bind to the tricyclic antidepressant binding site (*12*). Radioligand binding and photoaffinity labeling data also indicate that tricyclic antidepressants and PCP bind to overlapping sites (*29*, *40*, *41*). Complementary molecular docking studies helped in the localization of the potential binding sites for fluoxetine in each particular neuronal AChR subtype (see Figure 3B−D). The analysis of the obtained molecular complexes indicates that fluoxetine in either the neutral or protonated form binds to the middle portion of the hα4β2 (Figure 3B), hα3β4 (Figure 3C), and hα7 (Figure 3D) AChR ion channels in a domain formed by amino acid rings numbered from the cytoplasmic end at positions 6′ and 13′. The binding site location of fluoxetine determined by molecular docking, in particular in the hα3β4 AChR, coincides with the "electrical distance" (0.42 ± 0.05) for the action of fluoxetine in the α3β4 ion channel estimated by voltage-clamp studies, suggesting that SSRIs inhibit ion flux by binding to a site located approximately in the middle of the ion channel (*5*).

In a comparable work, the binding of fluoxetine was analyzed in the *Torpedo* AChR ion channel (*12*), and similar results were observed for the neutral state of fluoxetine where it also binds between amino acid rings at positions 9′ and 13′. Nevertheless, the binding site location for protonated fluoxetine depended on the docking method used. The binding site for protonated fluoxetine determined by binding energy scoring (i.e., BE protonated) was found at positions 20′ and 24′, whereas the binding site location determined by Ludi scoring (i.e., Ludi protonated) was found at positions 9′ and 13′. Using our methodology, we docked fluoxetine into the *Torpedo* AChR ion channel model, and the results indicate that fluoxetine binds at positions 9′, 13′, and 17′ (data not shown), which is similar to the case of docking to the neuronal hα4β2, hα3β4, and hα7 AChRs (Figure 3).

Considering the results described above as well as data from other laboratories, we envision a dynamic model in which SSRIs

may interact initially with the resting ion channel (e.g., see ref *9*), decreasing the probability of ion channel opening after ACh activation. The fraction of ACh-activated ion channels is subsequently decreased by accelerating the desensitization process (e.g., see refs *5* and *12*). Finally, SSRIs can block ion channels by interacting with a domain formed between the amino acid rings at positions 6′ and 13′. Similar mechanisms of noncompetitive inhibition and binding site location were described for tricyclic antidepressants (*24*, *25*, *29*, *40*, *42*) and for bupropion (*26*) (reviewed in refs *13* and *16*), suggesting a more general mode of inhibition elicited by structurally and functionally different antidepressants. Although these results do not directly address the antidepressant activity of SSRIs, they will pave the way for a better understanding of how these antidepressants interact with neuronal-type AChRs.

ACKNOWLEDGMENT

We thank Paulina Iacoban for her technical assistance.

REFERENCES

1. National Institute of Mental Health (2008) Depression. Publication 08 3561, pp 1−25 (www.nimh.nih.gov).
2. Levinson, D. F. (2006) The genetics of depression: A review. *Biol. Psychiatry 60*, 84–92.
3. Peterson, B. S., Warner, V., Bansal, R., Zhu, H., Hao, X., Liu, J., Durkin, K., Adams, P. B., Wickramaratne, P., and Weissman, M. M. (2009) Cortical thinning in persons at increased familial risk for major depression. *Proc. Natl. Acad. Sci. U.S.A. 106*, 6273–6278.
4. Baldessarini, R. J. (2001) Drugs and the treatment of psychiatric disorders. In Goodman & Gilman's The pharmacological basis of therapeutics (Hardman, J. G., and Limbird, L. E., Eds.) 10th ed., pp 447−483, McGraw-Hill, New York.
5. García-Colunga, J., Awad, J. N., and Miledi, R. (1997) Blockage of muscle and neuronal nicotinic acetylcholine receptors by fluoxetine (Prozac). *Proc. Natl. Acad. Sci. U.S.A. 94*, 2041–2042.
6. García-Colunga, J., Vázquez-Gómez, E., and Miledi, R. (2004) Combined actions of zinc and fluoxetine on nicotinic acetylcholine receptors. *Pharmacogenomics J. 4*, 388–393.
7. García-Colunga, J., and Miledi, R. (1999) Blockage of mouse muscle nicotinic receptors by serotonergic compounds. *Exp. Physiol. 84*, 847–864.
8. López-Valdés, H. E., and García-Colunga, J. (2001) Antagonism of nicotinic acetylcholine receptors by inhibitors of monoamine uptake. *Mol. Psychiatry 6*, 511–519.
9. Maggi, L., Palma, E., Miledi, R., and Eusebi, F. (1998) Effects of fluoxetine on wild and mutant neuronal α7 nicotinic receptors. *Mol. Psychiatry 3*, 350–355.
10. Fryer, J. D., and Lukas, R. J. (1999) Antidepressants noncompetitively inhibit nicotinic acetylcholine receptor function. *J. Neurochem. 72*, 1117–1124.
11. Feuerbach, D., Lingenhöhl, K., Dobbins, P., Mosbacher, J., Corbett, N., Nozulak, J., and Hoyer, D. (2005) Coupling of human nicotinic acetylcholine receptors α7 to calcium channels in GH3 cells. *Neuropharmacology 48*, 215–227.
12. Arias, H. R., Feuerbach, D., Bhumireddy, P., and Ortells, M. O. (2010) Inhibitory mechanisms and binding site locations for serotonin selective reuptake inhibitors on nicotinic acetylcholine receptors. *Int. J. Biochem. Cell Biol. 42*, 712–724.
13. Arias, H. R., Bhumireddy, P., and Bouzat, C. (2006) Molecular mechanisms and binding site locations for noncompetitive antagonists of nicotinic acetylcholine receptors. *Int. J. Biochem. Cell Biol. 38*, 1254–1276.
14. Arias, H. R. (2006) Ligand-gated ion channel receptor superfamilies. In Biological and Biophysical Aspects of Ligand-Gated Ion Channel Receptor Superfamilies (Arias, H. R., Ed.) pp 1−25, Research Signpost, Kerala, India.
15. Albuquerque, E. X., Pereira, E. F. R., Alkondon, A., and Rogers, S. W. (2009) Mammalian nicotinic acetylcholine receptors: From structure to function. *Physiol. Rev. 89*, 73–120.
16. Arias, H. R. (2009) Is the inhibition of nicotinic acetylcholine receptors by bupropion involved in its clinical actions? *Int. J. Biochem. Cell Biol. 41*, 2098–2108.
17. Shytle, R. D., Silver, A. A., Lukas, R. J., Newman, M. B., Sheehan, D. V., and Sanberg, P. R. (2002) Nicotinic receptors as targets for antidepressants. *Mol. Psychiatry 7*, 525–535.
18. Picciotto, M. R., Brunzell, D. H., and Caldarone, B. J. (2002) Effect of nicotine and nicotinic receptors on anxiety and depression. *NeuroReport 13*, 1097–1106.
19. George, T. P., Sacco, K. A., Vessicchio, J. C., Weinberger, A. H., and Shytle, R. D. (2008) Nicotinic antagonist augmentation of selective serotonin reuptake inhibitor-refractory major depressive disorder. A preliminary study. *J. Clin. Psychopharmacol. 28*, 340–344.
20. Popik, P., Kozela, E., and Krawczyk, M. (2003) Nicotine and nicotinic receptor antagonists potentiate the antidepressant-like effects of imipramine and citalopram. *Br. J. Pharmacol. 139*, 1196–1202.
21. Caldarone, B. J., Hrrist, A., Cleary, M. A., Beech, R. D., King, S. L., and Picciotto, M. R. (2004) High-affinity nicotinic acetylcholine receptors are required for antidepressant effects of amitriptyline on behavior and hippocampal cell proliferation. *Biol. Psychiatry 56*, 657–664.
22. Polson, R. G., Fleming, P. M., and O'shea, J. K. (2004) Fluoxetine in the treatment of amphetamine dependence. *Hum. Psychopharmacol. Clin. Exp. 8*, 55–58.
23. Michelmore, S., Croskery, K., Nozulak, J., Hoyer, D., Longato, R., Weber, A., Bouhelal, R., and Feuerbach, D. (2002) Study of the calcium dynamics of the human α4β2, α3β4 and α1β1γδ nicotinic acetylcholine receptors. *Naunyn-Schmiedeberg's Arch. Pharmacol. 366*, 235–245.
24. Arias, H. R., Targowska-Duda, K. M., Sullivan, C. J., Feuerbach, D., Maciejewski, R., and Jozwiak, K. (2010) Different interaction between tricyclic antidepressants and mecamylamine with the human α3β4 nicotinic acetylcholine receptor. *Int. Neurochem. 56*, 642–649.
25. Arias, H. R., Rosenberg, A., Targowska-Duda, K. M., Feuerbach, D., Jozwiak, K., Moaddel, R., and Weiner, I. W. (2010) Tricyclic antidepressants and mecamylamine bind to different sites in the human α4β2 nicotinic receptor ion channel. *Int. J. Biochem. Cell Biol. 42*, 1007–1018.
26. Arias, H. R., Gumilar, F., Rosenberg, A., Targowska-Duda, K. M., Feuerbach, D., Jozwiak, K., Moaddel, R., Wainer, I. W., and Bouzat, C. (2009) Interaction of bupropion with muscle-type nicotinic acetylcholine receptors in different conformational states. *Biochemistry 48*, 4506–4518.
27. Moore, M. A., and McCarthy, M. P. (1995) Snake venom toxins, unlike smaller antagonists, appear to stabilize a resting state conformation of the nicotinic acetylcholine receptor. *Biochim. Biophys. Acta 1235*, 336–342.
28. Cheng, Y., and Prusoff, W. H. (1973) Relationship between the inhibition constant (K_i) and the concentration of inhibitor which causes 50% inhibition (IC_{50}) of an enzymatic reaction. *Biochem. Pharmacol. 22*, 3099–3108.
29. Sanghvi, M., Hamouda, A. K., Jozwiak, K., Blanton, M. P., Trudell, J. R., and Arias, H. R. (2008) Identifying the binding site(s) for antidepressants on the *Torpedo* nicotinic acetylcholine receptor: [^{3}H]2-Azidoimipramine photolabeling and molecular dynamics studies. *Biochim. Biophys. Acta 1778*, 2690–2699.
30. Unwin, N. (2005) Refined structure of the nicotinic acetylcholine receptor at 4 Å resolution. *J. Mol. Biol. 346*, 967–989.
31. Miyazawa, A., Fujiyoshi, Y., and Unwin, N. (2003) Structure and gating mechanism of the acetylcholine receptor pore. *Nature 423*, 949–955.
32. Gerzanich, V., Peng, X., Wang, F., Wells, G., Anand, R., Fletcher, S., and Lindstrom, J. (1995) Comparative pharmacology of epibatidine: A potent agonist for neuronal nicotinic acetylcholine receptors. *Mol. Pharmacol. 48*, 774–782.
33. DeVane, C. L. (1999) Metabolism and pharmacokinetics of selective serotonin reuptake inhibitors. *Cell. Mol. Neurobiol. 19*, 443–466.
34. Karson, C. N., Newton, J. E., Livingston, R., Jolly, J. B., Cooper, T. B., Sprigg, J., and Komoroski, R. A. (1993) Human brain fluoxetine concentrations. *J. Neuropsychiatry Clin. Neurosci. 5*, 322–329.
35. Bolo, N. R., Hodé, Y., Nédélec, J., Lainé, E., Wagner, G., and Macher, J. (2000) Brain pharmacokinetics and tissue distribution *in vivo* of fluvoxamine and fluoxetine by fluorine magnetic resonance spectroscopy. *Neuropsychopharmacology 23*, 428–438.
36. Glick, S. D., Sell, E. M., and Maisonneuve, I. M. (2008) Brain regions mediating α3β4 nicotinic antagonist effects of 18-MC on methamphetamine and sucrose self-administration. *Eur. J. Pharmacol. 599*, 91–95.
37. Grady, S. R., Moretti, M., Zoli, M., Marks, M. J., Zanardi, A., Pucci, L., Clementi, F., and Gotti, C. (2009) Rodent habenulo-interpeduncular pathway expresses a large variety of uncommon nAChR subtypes, but only the α3β4* and α3β3β4* subtypes mediate acetylcholine release. *J. Neurosci. 29*, 2272–2282.

38. Gotti, C., Zoli, M., and Clementi, F. (2006) Brain nicotinic acetylcholine receptors: Native subtypes and their relevance. *Trends Pharmacol. Sci. 27*, 482–491.
39. DeBiasi, M., and Salas, R. (2008) Influence of neuronal nicotinic receptors over nicotine addiction and withdrawal. *Exp. Biol. Med. 233*, 917–929.
40. Gumilar, F., Arias, H. R., Spitzmaul, G., and Bouzat, C. (2003) Molecular mechanism of inhibition of nicotinic acetylcholine receptors by tricyclic antidepressants. *Neuropharmacology 45*, 964–976.
41. Hamouda, A. K., Chiara, D. C., Blanton, M. P., and Cohen, J. B. (2008) Probing the structure of the affinity-purified and lipid-reconstituted *Torpedo* nicotinic acetylcholine receptor. *Biochemistry 47*, 12787–12794.
42. Gumilar, F., and Bouzat, C. (2008) Tricyclic antidepressants inhibit homomeric Cys-loop receptors by acting at different conformational states. *Eur. J. Pharmacol. 584*, 30–39.